# Influence of magnetic field on flame dynamics in hydrogen flames: A numerical study

Mysore Natesh, V.; Langella, I.

**DOI**
10.1016/j.proci.2025.105892

**Publication date**
2025

**Document Version**
Final published version

**Published in**
Proceedings of the Combustion Institute

Proceedings of the Combustion Institute 41 (2025) 105892

Contents lists available at ScienceDirect

Proceedings of the Combustion Institute

journal homepage: www.elsevier.com/locate/proci

# Influence of magnetic field on flame dynamics in hydrogen flames: A numerical study

Vaibhav Mysore Natesh *, Ivan Langella

*Faculty of Aerospace Engineering, TU Delft, Kluyverweg 1, Delft, 2629 HS, The Netherlands*

ARTICLE INFO

*Keywords:*
Magnetic field effects
Hydrogen combustion
Swirl-stabilized flame
Paramagnetic species

ABSTRACT

Electromagnetic fields influence flame behavior by altering the transport of paramagnetic species such as oxygen and OH radicals in hydrogen flames, affecting reaction pathways and combustion dynamics. This study presents a numerical investigation of the effects of magnetic fields on a premixed swirl-stabilized hydrogen flame using a modified combustion solver in OpenFOAM. Additional body force and diffusion terms were incorporated into the governing equations to model interactions with paramagnetic species, and the solver was validated against experimental data and simulations from the literature. The study focuses on analyzing flame structure, species redistribution, and mixture fraction variations under magnetic conditioning. Large Eddy Simulations (LES) with the Eulerian Stochastic Fields (ESF) method were employed to capture turbulence-chemistry interactions. The results indicate that the presence of a magnetic field induces an upstream-directed force on oxygen, leading to localized changes in mixture fraction and combustion characteristics. A reduction in temperature, heat release rate, and OH concentration was observed, with peak reductions of approximately 2%, 5%, and 6%, respectively. These effects are attributed to the redistribution of oxygen, which makes the flame locally leaner. This study extends the understanding of hydrogen combustion under electromagnetic influence and demonstrates the potential of magnetic fields for controlling the flame behavior. The findings provide new insights into magnetic field-assisted combustion strategies, offering a framework for further research in advanced propulsion and energy applications.

## 1. Introduction

The urgent need for sustainable energy solutions has driven global efforts to transition from conventional fossil fuels to cleaner and more efficient alternatives. Hydrogen combustion is considered a promising pathway toward carbon-neutral energy systems, as it produces only water vapor when combusted. However, hydrogen flames present several challenges, including high flame temperatures, which lead to increased NOx emissions, and instability due to its high diffusivity and reactivity. Addressing these issues is crucial for the practical implementation of hydrogen as a primary fuel in industrial and power generation applications.

Flames are known to exhibit responsiveness to magnetic fields. Previous research has explored various approaches to controlling hydrogen combustion characteristics, with electromagnetic fields emerging as a potential solution. Magnetic fields have been shown to influence combustion processes by acting on paramagnetic species such as oxygen $O_2$ and hydroxyl radicals OH. Studies have demonstrated that these interactions can modify the flame structure, enhance stability, and even suppress emissions through controlled radical redistribution. The fundamental mechanism behind this influence lies in the differential response of paramagnetic species to magnetic forces, which induces changes in convection, diffusion, and reaction rates within the flame.

The application of magnetic fields in combustion science has been investigated in both experimental and numerical studies. Kajimoto et al. [1] demonstrated that magnetic forces indirectly affect OH radical distribution by acting on surrounding paramagnetic oxygen, altering convection patterns and thereby modifying flame characteristics. Yamada et al. [2] extended this analysis to hydrogen-oxygen diffusion flames, confirming that magnetic fields could significantly impact flame structure through changes in species transport. Furthermore, Fujita et al. [3] explored the effect of magnetic fields on diffusion flames under microgravity, showing that flame shape and emission characteristics could be actively controlled by adjusting the field strength. These studies collectively suggest that magnetic fields have the potential to improve combustion control and efficiency.

Most prior studies have focused on methane-air flames, with limited investigations into hydrogen flames, which have different chemical and transport properties. Furthermore, most of these studies have

* Corresponding author.
*E-mail address:* v.mysorenatesh@tudelft.nl (V. Mysore Natesh).

https://doi.org/10.1016/j.proci.2025.105892
Received 1 May 2025; Accepted 21 September 2025
Available online 9 October 2025

been conducted under laminar conditions, which are rare in practical applications where turbulent effects dominate combustion behavior. Additionally, while NOx suppression through strain has been demonstrated [4], the role of magnetic fields in influencing strain-driven NOx reduction remains unexplored. Hydrogen flames, particularly in swirled configurations [5,6] are highly sensitive to turbulence, differential diffusion effects, and strain-induced modifications in radical distribution. Understanding how magnetic fields interact with these factors is critical for developing advanced combustion strategies.

The present study aims to address these gaps by numerically investigating the effect of magnetic fields on a swirled-stabilized hydrogen flame. In this study, LES with transport PDF in the framework of ESF incorporating the effects of magnetic fields is carried out. Additional body force and diffusion terms are introduced to model interactions between paramagnetic species and magnetic fields in turbulent flow and chemistry interactions. The study builds upon previous experimental findings by extending the analysis to high-fidelity numerical simulations, providing insights into radical redistributions in a swirl stabilized flame.

## 2. Governing equations

### 2.1. Magnetic body force

The external force acting on paramagnetic species in the presence of a magnetic field is given by :

$$f_i = \frac{1}{2\mu_0}\chi_i \nabla B^2 \tag{1}$$

where $f_i$ is the external force per unit mass acting on species $i$, $\mu_0$ is the vacuum permeability determining the medium's response to the applied magnetic field, $\chi_i$ is the magnetic susceptibility of species $i$ which quantifies the species' influence under the magnetic field, and $B$ is the magnetic flux density representing the strength of the applied magnetic field. The inclusion of this force term allows for the modeling of radical redistribution and its impact on combustion properties. Note that $f_i$ is distinct from the Lorentz force, which acts on ions and is neglected in this study due to its smaller order of magnitude compared to the force acting on paramagnetic species.

The temperature dependence of magnetic susceptibility is described by Curie's Law [2]:

$$\chi_i = \frac{N_A g_i^2 \mu_B^2 S_i(S_i+1)\mu_0}{3kTm_i} \tag{2}$$

where $N_A$ is Avogadro's number, $g_L$ is the Lande g-factor accounting for the coupling between an electron's spin and the applied magnetic field, $\mu_B$ is the Bohr magneton representing the fundamental unit of magnetic moment associated with an electron, $S_i$ is the total electron spin quantum number of species $i$ which determines its intrinsic magnetic moment, $\mu_0$ is the vacuum permeability describing the ability of free space to support a magnetic field, $k$ is the Boltzmann constant relating temperature to energy at the molecular scale, $T$ is the absolute temperature which inversely affects the magnetic susceptibility, and $m_i$ is the molecular mass of species $i$ influencing the strength of its magnetic response.

As temperature increases, the susceptibility $\chi$ decreases, reducing the influence of the magnetic force on species transport. This temperature dependence is critical in combustion modeling, as it affects the extent to which species transport is altered by applied magnetic fields.

### 2.2. Reacting flow equations

In this study, the open-source CFD software OpenFOAM [7] has been used. Large Eddy Simulations (LES) simulations have been conducted, as the LES approach captures the unsteady characteristics of turbulent flows while reducing the dependence on modeling assumptions. In fact, in LES, the large-scale motions are explicitly resolved, while the small-scale structures, smaller than a specified cut-off filter, are modeled. The cut-off filter is usually taken as $\Delta = \sqrt[3]{V_{cell}}$, where $V_{cell}$ is the volume of the local cell in the numerical mesh.

With this formulation, the Favre-filtered transport equations can be expressed as described in [8]:

$$\frac{\partial \overline{\rho}}{\partial t} + \frac{\partial \overline{\rho}\tilde{u}_i}{\partial x_i} = 0 \tag{3}$$

$$\frac{\partial \overline{\rho}\tilde{u}_i}{\partial t} + \frac{\partial \overline{\rho}\tilde{u}_i\tilde{u}_j}{\partial x_j} = -\frac{\partial \overline{p}}{\partial x_i} + \frac{\partial}{\partial x_j}\left(\overline{\tau_{ij}} - \overline{\rho}\left(u_i\tilde{u}_j - \tilde{u}_i\tilde{u}_j\right)\right) + \overline{\rho}\sum_{i=1}^{N} Y_i f_i \tag{4}$$

where $\tilde{u}_i$ represents the $i$th component of the filtered velocity, while $\overline{\rho}$ and $\overline{p}$ denote the filtered fluid density and pressure, respectively. The shear stress tensor $\overline{\tau_{ij}}$ for Newtonian fluids is approximated using the gradient diffusion hypothesis:

$$\overline{\tau_{ij}} = 2\overline{\mu}\left(\widetilde{S_{ij}} - \frac{1}{3}\delta_{ij}\widetilde{S_{kk}}\right)$$

where $\overline{\mu}$ is the filtered dynamic viscosity, $\widetilde{S_{ij}}$ represents the components of the favre filtered rate-of-strain tensor, and $\delta_{ij}$ is the Kronecker delta. The unresolved Reynolds stresses are modeled using the Boussinesq hypothesis as follows:

$$\tau_{sgs,ij} = \overline{\rho}\left(u_i\tilde{u}_j - \tilde{u}_i\tilde{u}_j\right)$$

$$\tau_{sgs,ij} = -2\mu_{sgs}\left(\widetilde{S_{ij}} - \frac{1}{3}\delta_{ij}\widetilde{S_{kk}}\right)$$

where $\mu_{sgs}$ is the eddy viscosity. Here, $f_i$ represents the body force in Eq. (1) due to the applied magnetic field.

The generic equation for the species mass fraction $Y_k$ reads:

$$\frac{\partial \overline{\rho}\widetilde{Y}_k}{\partial t} + \frac{\partial}{\partial x_i}\left(\overline{\rho}\tilde{u}_i\widetilde{Y}_k\right) = \frac{\partial}{\partial x_i}\left[\overline{\rho}D_k\left(\frac{\partial \widetilde{Y}_k}{\partial x_i} - \frac{m_k}{m}\frac{\overline{\rho}}{p}\sum_{j=1}^{N}\widetilde{Y}_k\widetilde{Y}_j\left(f_i - f_j\right)\right) + \frac{\mu_{sgs}}{Sc_t}\frac{\partial \widetilde{Y}_k}{\partial x_i}\right] - \overline{\dot{\omega}}_k \tag{5}$$

where $D_k$ is the diffusivity of species $k$, $Sc_t = 0.7$ is the subgrid Schmidt number and $\overline{\dot{\omega}}_k$ is the filtered reaction rate of species $k$, $m_k$ is the molar mass of species $k$, $m$ is the molar mass of the mixture and $p$ is the pressure. The effect of the magnetic field, second term on the RHS of Eq. (5), is incorporated as an additional diffusion term, arising from the difference in forces acting on different scalar species. Since radicals exhibit varying spin numbers, they experience distinct magnetic forces. This force disparity induces an additional diffusion effect in the species transport equations. An equation for the specific sensible enthalpy $\tilde{h}_s$ is also solved, which reads:

$$\frac{\partial \overline{\rho}\widetilde{h_s}}{\partial t} + \frac{\partial \overline{\rho}\tilde{u}_i\widetilde{h_s}}{\partial x_i} = \frac{\partial \widetilde{p}}{\partial t} + \tilde{u}_i\frac{\partial \widetilde{p}}{\partial x_i} + \widetilde{\omega_T} + \frac{\partial}{\partial x_i}\left(\left(\lambda + \frac{\mu_{sgs}c_{p,mix}}{Pr_t}\right)\frac{\partial \widetilde{T}}{\partial x_i}\right) - \frac{\partial}{\partial x_i}\left(\overline{\rho}\sum_{k=1}^{N}V_{k,i}\widetilde{Y_k}\widetilde{h_{s,k}}\right) + \overline{\rho}\sum_{k=1}^{N}\widetilde{Y_k}f_k\cdot V_{k,i} \tag{6}$$

with $N$ being the number of species, $Pr_t = 0.7$ the subgrid Prandtl number, $\widetilde{\omega_T}$ the heat release rate and $\widetilde{h_{s,k}}$ the sensible enthalpy of species k. Mixture thermal conductivity $\lambda$ and dynamic viscosity $\mu$ are computed using Sutherland transport law, while the mixture specific heat at constant pressure, $c_{p,mix}$, is computed from JANAF polynomials. The laminar species diffusion coefficient $D_k$ and the diffusion velocity $V_k, i$ are obtained assuming constant Lewis number and Fick's law respectively:

$$Le_k = \frac{\lambda}{\overline{\rho}c_{p,mix}D_k}$$

$$\widetilde{Y_k}V_{k,i} = -D_k\left(\frac{\partial\widetilde{Y_k}}{\partial x_i} - \frac{m_k}{m}\frac{\overline{\rho}}{p}\sum_{j=1}^{N}\widetilde{Y_k}\widetilde{Y_j}(f_i - f_j)\right)$$

Finally, ideal gas law is implemented to relate the density-varying mixture to temperature, pressure and composition.

To model the sub-grid stresses, the Wall-Adapting Local Eddy-viscosity (WALE) model [9] was used within the OpenFOAM solver.

### 2.3. Combustion modeling

In this study, a transported Probability Density Function (t-PDF) approach with Eulerian Stochastic Fields (ESF) is used. The equations are further modified to incorporate the effects of magnetic fields, enabling the study of their influence on combustion dynamics. The t-PDF with ESF formulation is provided below, follows an approach similar to that in [10]. The evolution of species and enthalpy is represented by the composition filtered density function (FDF), which accounts for their probability distribution under LES filtering. The fine-grained composition PDF $P_{sgs}(\psi) = \Pi_{\alpha=1}^{n}\delta(\psi_a - \phi_a)$, with $\alpha = 1,\ldots,n$ scalar quantities represented by $\phi_\alpha$, represents the probability of $\phi = \psi$. The FDF, or subgrid PDF, $\tilde{P}_{sgs}$, follows the transport equation:

$$\begin{aligned}
&\frac{\partial\overline{\rho}\tilde{P}_{sgs}}{\partial t} + \frac{\partial\overline{\rho}\tilde{u_j}\tilde{P}_{sgs}}{\partial x_j} + \sum_{\alpha=1}^{n}\frac{\partial}{\partial\psi_\alpha}\left(\overline{\rho}\dot{\omega}_\alpha\tilde{P}_{sgs}\right) = \\
&\frac{\partial}{\partial x_j}\left[\overline{\rho}\left(D_\alpha + D_t\right)\frac{\partial\tilde{P}_{sgs}}{\partial x_j}\right] \\
&-\frac{\partial}{\partial x_j}\left[k\tilde{P}_{sgs}\sum_{\beta=1}^{n}\phi_\beta(f_\alpha - f_\beta)\right] \\
&-\sum_{\alpha=1}^{n}\sum_{\beta=1}^{n}\frac{\partial^2}{\partial\psi_\alpha\psi_\beta}\left(\overline{\rho}\frac{\overline{\nu}}{Sc}\overline{\frac{\partial\phi_\alpha}{\partial x_i}\frac{\partial\phi_\beta}{\partial x_i}}|_{\phi=\psi}\tilde{P}_{sgs}\right)
\end{aligned} \tag{7}$$

The left-hand side (LHS) of the equation above includes the temporal evolution, convective transport, and chemical source term, respectively. The first term on the right-hand side (RHS) is the diffusion term, which consists of both laminar ($D$) and turbulent ($D_t$) contributions. The laminar diffusion term is modeled using a constant Lewis number approach to account for differential diffusion effects.

Here, the coefficient $k$ is a constant that accounts for molar mass density and pressure effects. Notably, this term is only applied to scalar quantities associated with species transport. For the enthalpy field, which is also a scalar, this term is omitted. Instead, a source term is introduced, which signifies work done due to the presence of magnetic forces, computed as the summation of the products of the force $f$ and the diffusion velocities, which is obtained after solving the species transport equations.

The final term on the RHS of Eq. (7) corresponds to molecular (micro-) mixing, which can be described using the Interaction by Exchange with the Mean (IEM) model [11], also referred to as the Linear Mean Square Estimate (LMSE) approach [12].

In the ESF method, the FDF is decomposed into $N_s$ stochastic fields, with $\zeta_\alpha^n$ being the $n$th realization of the scalar $\phi_\alpha$. In particular, following the method proposed by Valiño et al. [13], $\zeta_\alpha^n$ is described by:

$$\begin{aligned}
&d\overline{\rho}\zeta_\alpha^n + \frac{\partial(\overline{\rho}\tilde{u_i}\zeta_\alpha^n)}{\partial x_j}dt - \frac{\partial}{\partial x_j}\left[\left(D + D_t\right)\frac{\partial\zeta_\alpha^n}{\partial x_j}\right]dt = \\
&\overline{\rho}\sqrt{\frac{2\mu_{sgs}}{\overline{\rho}Sc_{sgs}}}\frac{\partial\zeta_\alpha^n}{\partial x_j}dW_j^n - \frac{\overline{\rho}}{2\tau_{sgs}}(\zeta_\alpha^n - \tilde{\phi}_\alpha)dt - \overline{\rho}\dot{\omega}_\alpha^n dt \\
&-\frac{\partial}{\partial x_j}\left[\overline{\rho}D\frac{m_\alpha\overline{\rho}}{mp}\sum_{\beta=1}^{N}\zeta_\beta^n(f_\alpha - f_\beta)\right]
\end{aligned} \tag{8}$$

The last term in the equation above captures the effects of magnetic fields, with $m_\alpha$ and $m$ representing molar mass of the scalar corresponding to species and mixture's molar mass.

It is important to note that each stochastic field solution does not represent a physical realization of the actual field. Instead, it serves as an equivalent stochastic system to Eq. (7). The filtered scalar value can then be reconstructed using the following expression:

$$\tilde{\phi}_\alpha = \frac{1}{N}\sum_{n=1}^{N_s}\zeta_\alpha^n$$

The source of stochasticity of the field can be found in the Wiener process $dW_j^n$, resulting from the Itô integration of the Stochastic Partial Differential Equation (SPDE), hereby approximated by the time-step increment as:

$$dW_j^n = \gamma_j\sqrt{dt}$$

With $\gamma_j = \{-1, 1\}$ being a random dichotomic vector with zero mean.

## 3. Methodology

### 3.1. Computational details

The Navier–Stokes equations are discretized using the finite volume approach and the low-Mach approximation in the software OpenFOAM. Spatial gradients are approximated using central schemes and total variation diminishing scheme for the divergence term in the momentum equation so to avoid numerical instabilities in the flame region. Time derivatives are discretized using a first-order implicit Euler scheme. The time step for the LES is chosen to have a maximum Courant number below 0.3 within the domain. The San Diego mechanism [14] with 10 species and 23 reactions is used for all simulations presented in this study. In this work, the magnetic body force is applied to all species. Paramagnetic species ($O_2$, OH, O, H, $HO_2$) are assigned non-zero spin, while diamagnetic species are treated with zero spin, consistent with physical theory and validation studies.

### 3.2. Validation case

The solver incorporating the additional terms to account for the magnetic field was first qualitatively validated against experimental data from the literature [2]. The validation case consists of a laminar diffusion flame in an oxy-fuel combustion environment, with an applied magnetic force that peaks at 0.52 $T$ near the nozzle exit and then decreases exponentially in the axial direction. This variation creates a downward magnetic field gradient, which slows down the paramagnetic $O_2$ and OH species against the direction of the flow. Additionally, the OH radical distribution is influenced by both molecular diffusion and bulk convection, driven by the presence of oxygen in the coflow as well as in the oxidizer stream. A sketch of the case showing inlet and boundary conditions, and the applied magnetic force, is presented in Fig. 1.

The case was simulated without subgrid terms on a 2D axisymmetric structured mesh with about 9000 cells, resulting in a cell length of 0.2 mm in the flame region. A mesh independence study has been further performed (not shown), indicating that results do not further vary when the mesh resolution increases. Results show consistency with findings in [2], where the regions of higher temperature and OH radicals migrate toward the center of the flame under the influence of the magnetic field. Contours of temperature difference between the cases without and with magnetic fields obtained from the computations are compared to experimental data in Fig. 1, and highlight the redistribution of thermal energy within the flame structure. Although a broader area of temperature difference is observed in the experiments, the numerical simulation captures the temperature variation range and its spatial distribution with reasonable accuracy. The formulation of the magnetic body force is consistent in both laminar and turbulent regimes, as it is based on species susceptibilities and field gradients, with its LES implementation supported by the validated ESF framework for turbulent combustion. The solver with magnetic force is thus retained for the analyses in the next section.

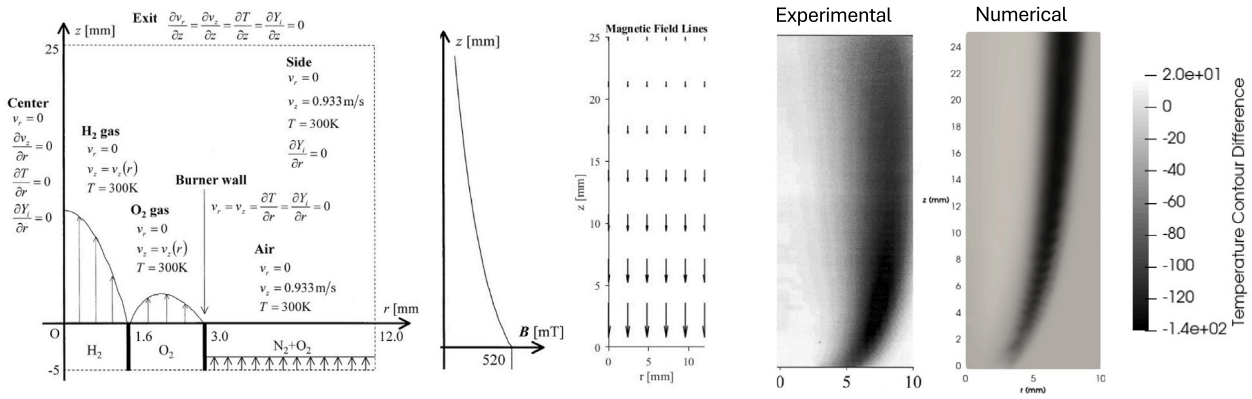


**Fig. 1.** Sketch of the numerical domain, with inlet, boundary conditions, applied magnetic force and field lines (left). Contours of temperature difference between cases with and without magnetic fields, obtained from experiments [2] and present computations (right).

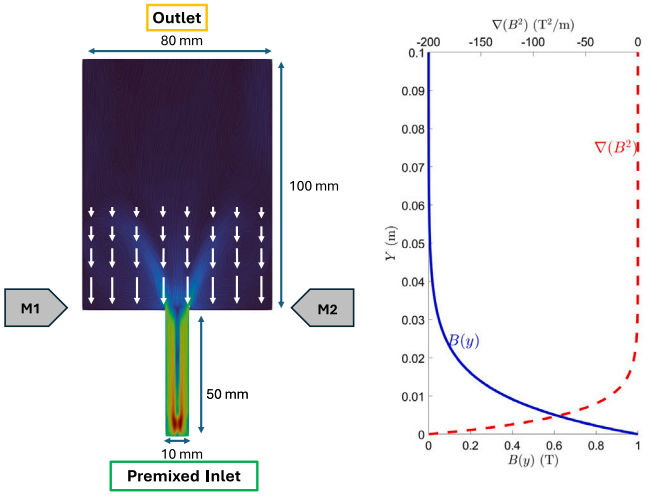


**Fig. 2.** Sectional view of the confined swirl-stabilized flame geometry (with magnetic field lines) and profile of magnetic fields.

### 3.3. Swirled flow case

A confined, swirl-stabilized premixed hydrogen-air flame is simulated at an equivalence ratio of 0.3. This choice is made to ensure a steady and well-defined combustion regime while preventing blow-off and flashback, which were observed for respectively lower and higher values. Moreover, differential diffusion effects are enhanced at very lean conditions, thus the present operating condition offers a way to study possible coupling between magnetic effect and differential diffusion, as will be shown later. The computational domain consists of a cylindrical geometry, designed to capture the flow dynamics and combustion characteristics under the influence of magnetic fields. Fig. 2 provides an overview of the geometry, including a sectional view with the relevant dimensions used for the numerical domain.

A swirl number $S$ is imposed on the flow and is defined as:

$$S = \frac{\int_0^{d_A/2} U_t U_a r^2 dr}{(d_A/2)\int_0^{d_A/2} U_a^2 r dr} \tag{9}$$

where $U_t$ and $U_a$ represent tangential and axial velocity components, respectively, at the nozzle exit plane. The term $d_A$ denotes the diameter of the nozzle. In this study, the inlet swirl number is set to 1.2 in order to ensure the formation of a central recirculation zone (CRZ), which enhances mixing and prolongs the residence time of reactants, thereby promoting efficient combustion. In swirl flows, regions of low velocity naturally form due to flow recirculation. These low-speed regions help maximize the influence of magnetic forces relative to convection. The resulting flow has a Reynolds Number (Re) ≈ 20000, which ensures a damped precessing vortex core (PVC), reducing large-scale flow oscillations and improving overall flow stability [5].

Inlet axial and tangential velocity components are determined using the specified swirl number, Reynolds number, and the cross-sectional area of the inlet. The boundary conditions are summarized in Table 1.

**Table 1**
Boundary conditions for the swirled flow case.

| Boundary | Condition |
|---|---|
| Inlet | Velocity inlet: $U_a = 30$ m/s, $U_t = 54$ m/s |
| Outlet | Pressure outlet |
| Walls | No-slip condition and zero gradient for scalars |

The magnetic field was configured such that the magnets were placed near the streamwise location where the flame anchors. This positioning ensures that the magnetic field intensity is maximized in the region where its influence on the flame dynamics is most significant. The maximum field intensity is set to 1 $T$ and decreases exponentially in the axial direction as shown in Fig. 2, presenting the distribution along the axial direction $y$ of both magnetic field intensity $B$ and its squared gradient $\nabla(B^2)$.

A mesh refinement study was conducted using two different mesh resolutions, a coarse mesh, consisting of 0.25 million elements, with a typical cell length in the flame region of $\Delta \approx 0.5$ mm, and a finer mesh with 1.2 million elements and a cell length of $\Delta \approx 0.2$ mm in the flame region. The latter ensures that Pope's criterion for 80% turbulent kinetic energy and the wall-resolved condition ($y^+ \approx 1$) are satisfied ($y^+$ being the wall-normal coordinate), and that at least two cells are present within the flame thickness. The 1.2 million cells mesh is thus retained for the analyses to be presented in the next section. The reactive LES were performed for two cases, respectively without and with magnetic force, in order to assess the influence of the latter on flame dynamics.

## 4. Results

Midplane contours of mean temperature, mean heat release rate (HRR), and instantaneous OH mass fraction are shown for the cases without (noM) and with (M) magnetic field in Fig. 3.

Results indicate that the magnetic force decreases the temperature, HRR and OH concentration in the nozzle exit region, where the flame stabilizes, of approximately 2%, 5%, and 6%, respectively. This is the region where both magnetic field strength and its gradient peak. This

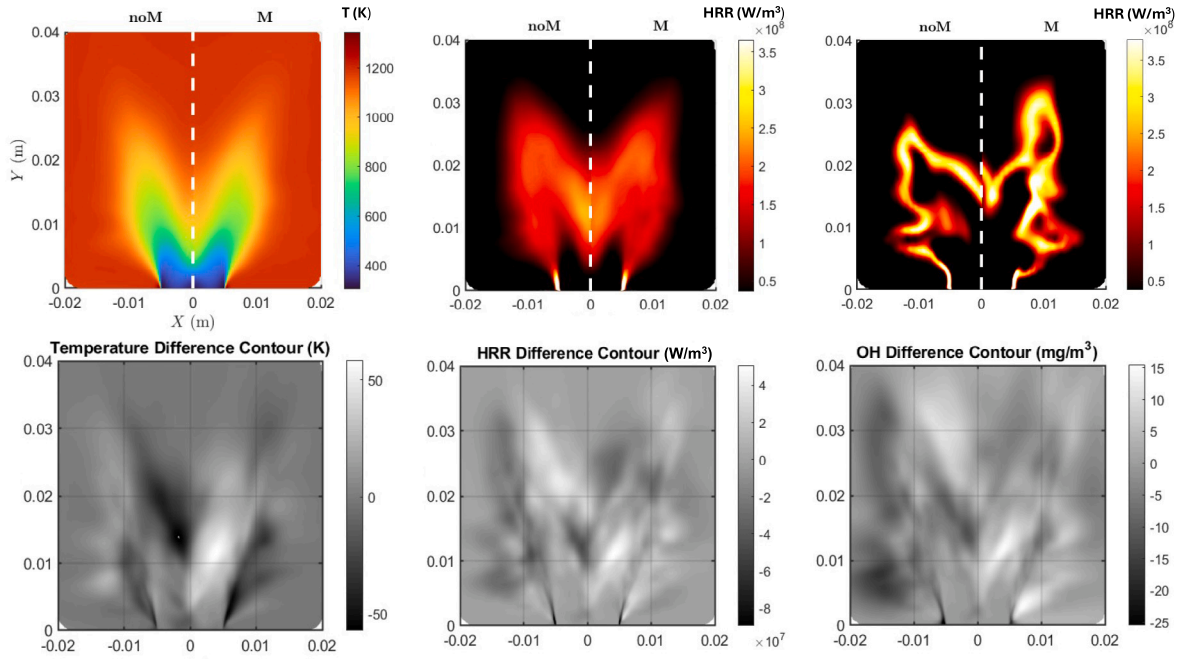


**Fig. 3.** Top: Midplane contours of mean temperature, mean heat release rate and instantaneous OH mass fraction without (noM) and with (M) magnetic fields. Bottom: Midplane contours of mean temperature, HRR and OH mass fraction difference between the M and noM cases.

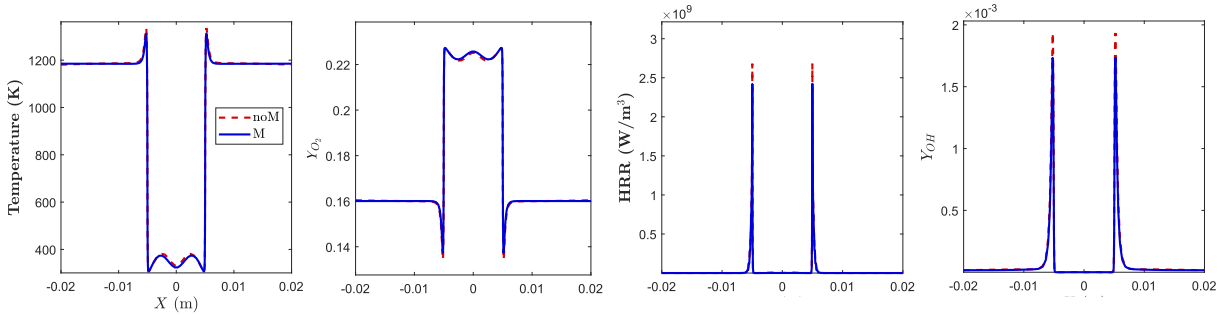


**Fig. 4.** Radial distribution of temperature, heat release rate (HRR), OH and oxygen mass fractions at an axial location $y = 0.1$ mm from the nozzle exit.

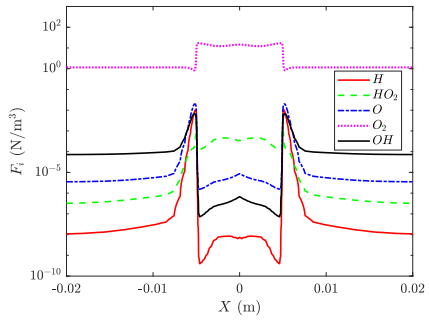


**Fig. 5.** Magnetic body force distribution for paramagnetic species at $y = 0.1$ mm.

effect is further marked by looking at the differences between noM and M cases for the three fields, also reported in the bottom of the figure.

To understand this effect, the forces acting on the paramagnetic species are analyzed in order to identify which species predominantly contributes to this behavior. Fig. 5 illustrates the distribution of magnetic body forces per unit volume, $F_i = \frac{1}{2\mu_0}\rho Y_i \chi_i \nabla(B^2)$, acting on various paramagnetic species $i$, at 0.1 mm distance from the nozzle exit.

It can be observed that the magnetic force is strongest in regions where the concentration of the species is high and where temperatures are relatively low. This behavior is expected, as the magnetic susceptibility of paramagnetic species increases at lower temperatures, enhancing their response to the applied magnetic field.

Among all species, $O_2$ experiences the highest magnetic force, with a magnitude of about three times that of other paramagnetic species. The forces acting on other radicals, such as OH and $HO_2$, are significantly weaker. As a result, their influence on the overall flame structure is minimal compared to oxygen. This suggests that any observed changes in flame behavior due to magnetic effects can primarily be attributed to the interaction of the magnetic field with molecular oxygen.

Further insight is provided by looking at the radial profiles of temperature, HRR, OH and $O_2$ mass fractions, shown in Fig. 4 for the same axial location $y = 0.1$ mm. At this location (where the magnetic force and gradients are strongest as discussed earlier), temperature, HRR, and OH concentration decrease in the presence of the magnetic field, consistently with the contours in Fig. 3. However, a localized

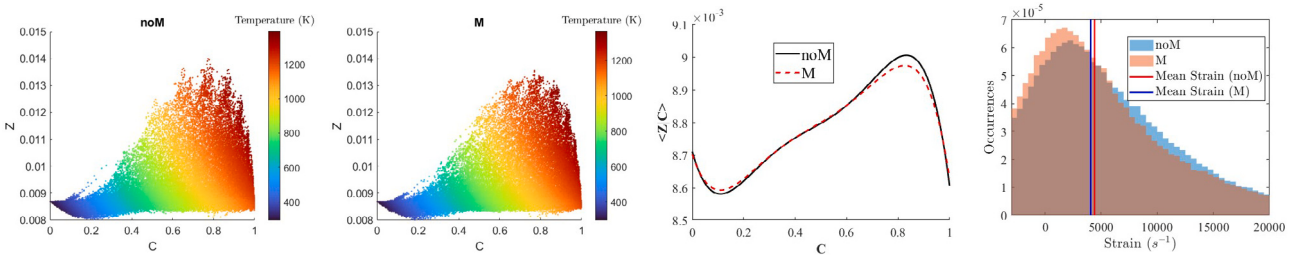


**Fig. 6.** From left to right: Scatter plots of mixture fraction $Z$ versus progress variable $c$ for the cases without (noM) and with (M) magnetic force; their conditional mean; and probability density function of mean strain for the noM and M cases. The vertical lines in the latter indicate the mean value.

rise in the peak mean oxygen concentration is noted, showing a 4% increase.

### 4.1. Mixture fraction analysis

To further investigate the effects of magnetic fields on the flame structure, a scatter plot of the progress variable $C$ versus the mixture fraction $Z$ is presented in Fig. 6. The mixture fraction is defined here using Bilger's expression:

$$Z = \frac{Z_H + \nu\left(Y_{O_2,\text{air}} - Z_0\right)}{1 + \nu Y_{O_2,\text{air}}}, \tag{10}$$

where the stoichiometric coefficient $\nu$ is determined by the ratio of the molar masses of oxygen and hydrogen as $\nu = 2M_{H_2}/M_{O_2}$, $Z_H$ and $Z_0$ represent the elemental mass fractions of hydrogen and oxygen, respectively, and $Y_{O_2,\text{air}}$ denotes the mass fraction of oxygen in air. The progress variable is defined as $C = 1 - Y_{H_2}/Y_{H_2,u}$, where $Y_{H_2,u}$ represents the unburned mass fraction of hydrogen. Note that, being this a premixed case, the mixture fraction varies due to differential diffusion effects. The comparison between the scatter plots for the cases with and without magnetic fields shown in the figure reveals that the mixture fraction reaches higher peaks in the case without magnetic field. This variation can be attributed to a localized increase in oxygen concentration, as was observed earlier, but also a decrease in the strain acting on the flame, resulting from the body force acting against the flow. This is also shown by looking at the strain rate distribution in the flame region, also shown in Fig. 6. The strain rate computation methodology follows the approach described in [15]. The strain rate is particularly high in the flame anchoring region due to the presence of shear layers formed at the interface between the central jet and the surrounding coflow. In particular, the increase of equivalence ratio as compared to the nominal value is a consequence of the coupling between strain rate and differential diffusion in hydrogen flames, as the equivalence ratio can only decrease without stretch (strain or curvature) effects [4]. When the magnetic field is introduced, the mean strain rate is reduced, which is attributed to the body force acting against the flow, which modifies the velocity field and relaxes the shear-induced strain. The combined effect of magnetic field, strain and differential diffusion causes at this point a decrease of mixture fraction in the region where the heat release rate is expected to peak ($C \approx 0.8$). This is shown by the conditional mean of $Z$ reported in Fig. 6, and is due to the fact that the nominal equivalence ratio $\phi = 0.3$ corresponds to negative Markstein length, for which an increase of tangential strain on the flame causes an increase of mixture fraction and vice versa. The presence of the magnetic fields seems to counteract this effect by locally increasing the oxygen concentration and reducing the strain, thereby shifting the conditional mean toward lower values. This aspect is of particular relevance as it implies that magnetic conditioning can be used as auxiliary mechanism to limit the occurrence of super-adiabatic temperatures and increase of flame speed in strained premixed hydrogen flames, which in turn can help reducing NOx emissions and preventing unwanted flashback.

## 5. Conclusions

Large Eddy Simulations of a swirl-stabilized premixed hydrogen-air flame at a nominal equivalence ratio of 0.3 have been performed using the Eulerian Stochastic Fields (ESF) method. Additional terms have been introduced to incorporate the effects of magnetic fields, and the solver has been validated against previous experimental data.

Results show that introducing a magnetic field leads to reductions in temperature, heat release rate, and OH concentration, particularly in the region of anchoring of the flame. These reductions, approximately 2%, 5%, and 6%, respectively, are attributed to the downward magnetic body force acting on paramagnetic diatomic oxygen. An analysis on radial profiles further indicates that the magnetic force leads to locally higher oxygen concentrations, resulting in a locally leaner flame. In particular, a coupling between strain, differential diffusion and magnetic force is observed. The magnetic force reduces the strain level, which due to the negative Markstein length at the explored conditions, in turns yields a peak decrease in mixture fraction. Thus, magnetic conditioning is effective in limiting super-adiabatic temperatures and (by limiting the increase of mixture fraction with strain) flame speed in turbulent premixed hydrogen flames, despite the relatively low magnetic force imposed, and might thus help the development of novel strategies to prevent flashback and suppress NOx emissions in premixed hydrogen flames.

## Novelty and significance statement

The novelty of this study lies in investigating the influence of magnetic fields on hydrogen combustion in a pre- mixed swirl-stabilized flame, an area that remains largely unexplored. This research extends the existing under- standing of paramagnetic species transport by incorporating magnetic force effects into Large Eddy Simulations using the Eulerian Stochastic Fields (ESF) method. The findings highlight the impact of the magnetic field on flame structure, species redistribution, and mixture fraction, particularly, a coupling between magnetic conditioning and differential diffusion is observed and discussed for the first time. The study provides new insights into magnetic field-assisted combustion control, offering a potential strategy for enhancing flame stability and reaction dynamics in propulsion and energy systems.

## CRediT authorship contribution statement

**Vaibhav Mysore Natesh:** Writing – original draft, Investigation, Formal analysis. **Ivan Langella:** Writing – review & editing, Supervision, Conceptualization.

## Declaration of competing interest

The authors declare that they have no known competing financial interests or personal relationships that could have appeared to influence the work reported in this paper.

## Acknowledgments

This project has received funding from the European Union's Horizon Europe Research and Innovation Programme under grant agreement No. 101120321, project ICHAruS. This work used the Dutch national e-infrastructure with the support of the SURF Cooperative using grant no. EINF-12170.

## References

[1] M.S. Tsuyoshi Kajimoto, K. Kitagawa, Dependence of magnetically induced change in oh distribution in a methane-air premixed flame on equivalence ratio, Combust. Sci. Technol. 175 (9) (2003) 1611–1623.
[2] E. Yamada, M. Shinoda, H. Yamashita, K. Kitagawa, Experimental and numerical analyses of magnetic effect on OH radical distribution in a hydrogen-oxygen diffusion flame, Combust. Flame 135 (4) (2003) 365–379.
[3] O. Fjita, K. Ito, T. Chida, S. Nagai, Y. TAKESHITA, Determination of magnetic field effects on a jet diffusion flame in a microgravity environment, Symp. (Int.) Combust. 27 (2) (1998) 2573–2578.
[4] A. Porcarelli, B. Kruljević, I. Langella, Suppression of NOx emissions by intensive strain in lean premixed hydrogen flamelets, Int. J. Hydrog. Energy 49 (2024) 413–431.
[5] N. Syred, J. Beér, Combustion in swirling flows: A review, Combust. Flame 23 (2) (1974) 143–201.
[6] S. Yu, X. Liu, X. Bai, A. Elbaz, W. Roberts, LES/PDF modeling of swirl-stabilized non-premixed methane/air flames with local extinction and re-ignition, Combust. Flame 219 (2020) 102–119.
[7] H.G. Weller, G. Tabor, H. Jasak, C. Fureby, A tensorial approach to computational continuum mechanics using object-oriented techniques, Comput. Phys. 12 (6) (1998) 620–631.
[8] P. Sagaut, Large Eddy Simulation for Incompressible Flows: an Introduction, Springer Science & Business Media, 2005.
[9] F. Nicoud, F. Ducros, Subgrid-scale stress modelling based on the square of the velocity gradient tensor, Flow, Turbul. Combust. 62 (3) (1999) 183–200.
[10] P. Breda, C. Yu, U. Maas, M. Pfitzner, Validation of an Eulerian stochastic fields solver coupled with reaction–diffusion manifolds on LES of methane/air non-premixed flames, Flow, Turbul. Combust. 107 (2021) 441–477.
[11] J. Villermaux, J. Devillon, Représentation de la coalescence et de la redispersion des domaines de ségrégation dans un fluide par un modèle d'interaction phénoménologique, in: Proceedings of the 2nd International Symposium on Chemical Reaction Engineering, vol. 26, Elsevier New York, 1972, pp. 1–13.
[12] C. Dopazo, E.E. O'Brien, An approach to the autoignition of a turbulent mixture, Acta Astronaut. 1 (9–10) (1974) 1239–1266.
[13] L. Valino, R. Mustata, K.B. Letaief, Consistent behavior of Eulerian Monte Carlo fields at low Reynolds numbers, Flow, Turbul. Combust. 96 (2016) 503–512.
[14] P. Saxena, F.A. Williams, Testing a small detailed chemical-kinetic mechanism for the combustion of hydrogen and carbon monoxide, Combust. Flame 145 (1–2) (2006) 316–323.
[15] L. Berger, A. Attili, H. Pitsch, Synergistic interactions of thermodiffusive instabilities and turbulence in lean hydrogen flames, Combust. Flame 244 (2022) 112254.